A High Resolution Tractography Phantom

Michael Bach[1,2], Klaus Fritzsche[3], Sena Minjoli[2], Bram Stieltjes[1], and Frederik Bernd Laun[1,2]

[1]Quantitative Imaging-based Disease Characterization, German Cancer Research Center, Heidelberg, Germany, [2]Dept. of Medical Physics in Radiology, German Cancer Research Center, Heidelberg, Germany, [3]Medical Imaging and Biological Informatics, German Cancer Research Center, Heidelberg, Germany

Introduction

The available diffusion phantoms can be divided into three main groups. Biological phantoms [1,2,3,4] are based on anisotropic biological tissue, artificially produced phantoms [5,6,7,8] use capillaries or fibers to generate anisotropic diffusion, and the third group are artificially generated data sets, the so called software phantoms [9,10,11].

While software phantoms can represent exactly defined structures, data distortion related to the real image-acquisition like eddy-currents, slice profiles or vibrations of the scanner are not taken into account or can be simulated to a limited extent. Using real phantoms, all these factors can be assessed in acquired data sets. Nonetheless, it is a great challenge to produce exactly defined, fine fiber strands of high resolution. Thus most of the available phantoms consist of fiber strands with diameters in the range of centimeters [5,6].

The aim of this work was to develop a diffusion phantom that is characterized by precisely defined and very fine structures and thus makes it possible to validate the whole diffusion tensor imaging (DTI)-pipeline from the data-acquisition to postprocessing schemes like denoising and fiber tracking.
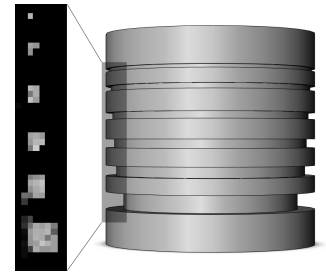
Fig.1. Left: High resolution FA map. Right: Phantom spindle

Materials and Methods

The phantom is made up of a plastic spindle (Polyoximethylene, POM) in which six grooves of a quadratic cross section are milled into (Fig. 1/right). Polyester fibers (diameter: 15 µm) are wound onto the spindle filling the grooves. A sodium chloride solution (83 g NaCl per 1 l water) is embedded between the polyester fibers. This solution has the same susceptibility as polyester and minimizes mesoscopic B_0-field variations [12].

Depending on the thread-tension and therefore on the packing density of the fibers, FA values of up to 0.9 can be reached. A homogenous pressure on the fibers and thus a uniform FA along the fiber strands (Fig. 2 b) is achieved by the circular cross section of the spindle. The cross sections of the grooves are 5x5 mm², 3x3 mm², 2.5x2.5 mm², 2x2 mm², 1.5x1.5 mm² and 1x1 mm² (Fig.1). The outer diameter of the spindle is 60 mm.

The distances between the grooves have been chosen such that a groove always starts at a multiple of 2.5 mm, measured from the beginning of the thickest groove. Hence, for a typical resolution (voxelsize) of 2.5 mm isotropic, the phantom can be adjusted so that every fiber strand starts in a new voxel. Therefore partial volume effects can be adjusted properly. The phantom is sealed with hot glue in order to prevent drying of the strands.

The measurements were performed on a 3 T MR scanner (Trio, Siemens, Erlangen, Germany) using a 32 channel head coil. A single-shot EPI with the following parameters was used. For the high resolution FA-map in Fig.1: FOV 240 mm, FOVphase 35 %, voxelsize $1x1x1$ mm³, TE 77 ms, TR 3400 ms, bandwidth 1158 Hz/px, b = 400 s/mm², 33 diffusions directions, 20 averages, GRAPPA acceleration factor 2.

For Fig.2: FOV 160 mm, FOVphase 75 %, voxelsize 2.5x2.5x2.5 mm³, TE 85 ms, TR 3100 ms, b = 850 s/mm², 33 diffusions directions, 10 averages, GRAPPA acc. factor 2.

Fiber tracking was performed with 3D-Slicer [13] using the following parameters: stopping mode FA 0.15, integration step length 1 mm, minimum path length 157 mm.
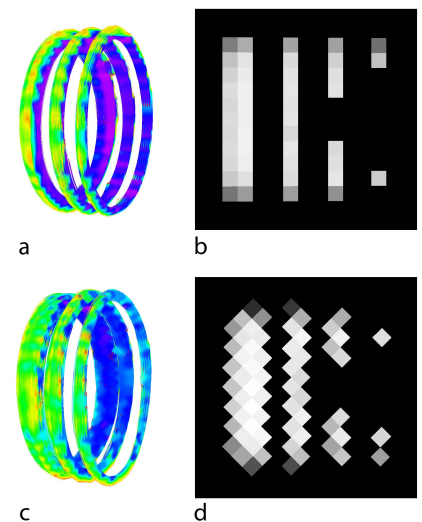
Fig.2. Fiber tracking result (a,c) and FA map (b,d). In (a,b), the fibers are aligned parallel to the voxels, and in (c,d), they are rotated by 45°. The resulting fiber tracts are thicker for the rotated field of view.

Results

In Fig. 1/left a fractional anisotropy (FA) map (voxelsize: 1x1x1 mm³) of the gray marked area is shown. The cross sectional areas of every fiber strand from 5x5 mm² down to just 1x1 mm² are clearly recognizable. The variations in the FA are mainly due to noise, whereas the reasons for small deviations from the actually quadratic shape are partial volume effects and EPI-distortions (phase-coded-direction from left to right).

Figure 2 shows FA-maps and fiber tracking results of the phantom with an isotropic resolution of 2.5 mm. Due to the too low resolution, the 3, 2.5 and 2 mm strands cannot be distinguished with respect to their thickness on the FA map (Fig. 2b). Because of their low signal, the two thinnest strands cannot be seen here. Fig. 2a/b and Fig. 2c/d were acquired with identical parameters, except for that the FOV was rotated by 45°. While in Fig. 2b the voxels are aligned with the fiber strands, the partial volume effects are more pronounced after the rotation. The effect of rotating the acquisition slice on fiber tracking is shown in Fig. 2 a/c. Before the rotation, the two thickest strands can clearly be distinguished, whereas this is hardly possible after the slice rotation by 45°. The FA along the fibers is represented by their color (violet: high FA, yellow: low FA).

Discussion

Using the here described production technique, a reliable and high-precision production of thin fiber strands (cross section area: 1 mm²) becomes possible. Additionally, the fiber strands provide a good FA-homogeneity along the whole strand. In comparison to simulations and software phantoms, the decisive advantage is, that the validation can be performed under real conditions. Due to these virtues, the phantom can be regarded as a good test model for diffusion weighted sequences (nominal and effective resolution, distortions), fiber tracking algorithms or other postprocessing schemes like TBSS.

References

[1] E. Sigmund et al., MRI 2005 [2] J. Lätt et al. Magn Reson Mater Phy 2007 [3] M.Descoteaux et al., MRM 2006 [4] J. Campbell et al. NeuroImage 2005 [5] E. Fieremans et al. JMR 2007 [6] C. Poupon et al., MRM 2008 [7] N. Yanasak et al., MRI 2006 [8] Moussavi et al. MRM 2010 [9] S. Barbieri NeuroImage 2011 [10] M. Bauer et al. Int J CARS (2011) [11] Delputte et al. ISMRM 2006 [12] Laun et al MRI 2009 [13] S.D. Pieper, M. Halle, R. Kikinis ISBI 2004